Asian Journal of
Earth Sciences

ISSN 1819-1886

Academic
Journals Inc.

www.academicjournals.com

Asian Journal of Earth Sciences 3 (2): 101-115, 2010
ISSN 1819-1886 / DOI: 10.3923/ajes.2008.62.76

Lunar Magnetic Pole Positions Deduced from High Albedo Magnetic Anomalies*

[1,2]M.C. Berguig, [1,2]M. Hamoudi, [1]Y. Cohen and [1]E. Thébault
[1]Institut de Physique du Globe de Paris, CNRS 4, Place jussieu 75005 Paris, France
[2]Université des Sciences et de Technologie, Alger BP 32,
El-Alia Bab Ezzouar, 16111 Algiers, Algeria

Abstract: The purpose of this research is to investigate the internal origin hypothesis by assuming that the crustal lunar magnetic field was generated by a paleo-dynamo process. The study is focused on four comparatively high intensity magnetic anomalies associated with high marked swirl albedo. These four formations: Reiner Gamma, Descartes Formation, Mare Marginis and Mare Ingenii, all having a similar Imbrian age, can also be fairly well modeled using simple magnetized disks at depth. Using these simple assumptions, the paleomagnetic pole positions have been determined. The modeling of these anomalies shows a cluster of paleomagnetic pole positions within a radius of about 35 degrees centered at (30S, 215E). These preliminary results are consistent with the hypothesis of a now extinct paleo-dynamo being responsible for magnetization of lunar crust. However, a more statistical analysis remains to be done over regions of weaker magnetic anomalies to be fully conclusive.

Key words: Albedo, magnetization, pole position, Descartes Formations, Mare Ingenii, Mare Marginis, Reiner Gamma

INTRODUCTION

It has been established that the Moon is lacking a global magnetic field (Ness, 1971) since the Explorer 35 mission at the end of 60's. However, the observations of solar wind interactions with the Moon revealed the existence of weak localized fields, which were later confirmed by in situ measurements (Dyal *et al*., 1974). In particular, a remnant magnetization could be estimated from the returned samples of the Apollo and Luna missions (Fuller, 1974). These measurements also suggested the existence of a past magnetizing field of about 100 μT around 3.9 Ga that decreased after 3.6 Ga (Cisowski *et al*., 1983; Collinson, 1993). Despite these informations, we do not have a clear idea concerning the internal or external origin of this past magnetizing field (Hood *et al*., 2001; Hood and Artemieva, 2008). The most straightforward analogy with the Earth's magnetic field is that the Moon once possessed a main magnetic field generated by a planetary dynamo that is now extinct (Fuller and Cisowski, 1987; Collinson, 1993). However, according to Hood and Huang (1991), the small size of the lunar core as derived from seismic data (Khan *et al*., 2004) and electromagnetic studies (Hood *et al*., 1999) would not be able to generate a dynamo sustaining a magnetic field with 100 μT amplitude. Instead, they invoke meteoric impacts in order to account for the relatively random nature of the lunar magnetic field (Hood and Huang, 1991), like over the Fra Mauro in the nearside (Hood *et al*., 1981), for instance. More recently, the hypothesis of magnetization acquired in the presence of transient fields generated by cometary impacts (Schultz and Snrka, 1980) has been revived by Richmond *et al*. (2005) who correlated strong anomalies with zones of high swirl albedo. However,

Corresponding Author: M.C. Berguig, Institut de Physique du Globe de Paris, CNRS 4, Place jussieu 75005 Paris, France Tel: +33 1 44 27 24 05 Fax: +33 1 44 27 74 63

*Originally Published in Asian Journal of Earth Sciences, 2008

this hypothesis seems to also be deficient for regions like Reiner Gamma (Nicholas *et al*., 2007) and Descartes Formation, for instance. For this latter zone, an albedo spectral analysis concluded that the material was not of exotic composition (Blewett *et al*., 2005). The debate is thus still open. Despite the random nature of the Moon magnetic field, recent measurements showed some disparities. Lunar Prospector (LP) reflectometer data have pointed out that the crustal rocks of the Moon were strongly demagnetized by meteoric impacts (Halekas *et al*., 2002), which makes it difficult to determine the origin of these magnetic anomalies. However, since the Apollo era, it has also been established that some lunar formations, like those located at the antipodes of the impact generated young basins, acquired relatively strong magnetization (Lin *et al*., 1998; Halekas *et al*., 2001; Hood *et al*., 2001). In addition, it has been noticed that high albedo features such as Reiner Gamma, Mare Ingenii, Mare Marginis and Descartes Formation are associated with strong magnetic anomalies (Hood and Schubert, 1980; Hood *et al*., 1981). This is confirmed by the accurate LP data (Hood *et al*., 2001; Richmond *et al*., 2003, 2005).

In this research, we take the opportunity of such clear and comparatively strong signals to test the existence of a former lunar dynamo. We focus our study on the strong magnetic anomalies associated with very marked albedo zones such as Reiner Gamma, Descartes Formation, Mare Marginis (located in the nearside of Moon) and Mare Ingenii (located in the farside of the Moon). These four regions are of similar Imbrian age of about 3.8 Ga (Richmond *et al*., 2003). Using an equivalent source method, we evaluate the magnetic signal generated by disks uniformly magnetized and we estimated the corresponding paleo-pole positions. We then discuss our obtained result and their limits.

DATA SELECTION AND PROCESSING

During the Apollo era only small regions within about 30 degrees of the lunar equator were magnetically mapped from orbit. In the Apollo 15 case, mainly two areas above Gerasimovich and Van de Graaff-Aitken in the farside were surveyed (Hood *et al*., 1981) while the Apollo 16 mission operated only over a very narrow nearside equatorial band. In contrast, the aim of the Lunar Prospector (LP) mission, whose lifetime was extended from January 1998 to the end of July 1999, was to globally map geophysical and geochemical properties of the Moon. Instruments and orbital parameters were chosen accordingly (Binder, 1998). A comprehensive description of the LP mission can be found in Andolz *et al*. (1998).

The data sets used in this study are the level 1 refined magnetometer data of the LP mission. However, the proximity of the solar maximum made it challenging to select the most undisturbed data. In order to maximize the signal to noise ratio, we only consider low altitude measurements, below 35 km, when the Moon is in the Earth's magnetic tail. This situation happened only 4 days per month during the LP's 19-month lifetime. High altitude data, acquired between 110 to 80 km during the year 1998, were discarded as they showed a signal that was comparatively too weak and of low resolution. This initial data selection drastically decreased the amount of usable data to about 7% of the whole database. The selected magnetometer data given in selenographic centered cartesian coordinate, were projected into spherical North, East and Radial components.

Despite the great care taken to select the data, high frequency external signals remain. A low-pass filter, based on Discrete Wavelet Transform (DWT) algorithms, was used to clean magnetic variations smaller than 10 km along the satellite tracks. This transformation method is described by Daubechies (1992) and has been previously applied to terrestrial magnetometer measurements (Fedi and Quarta, 1998; Leblanc and Morris, 2001). The anomaly field direction is not influenced much by these transformations. An example of the filtering is shown in Fig. 1.

The satellite data also contains a low frequency external signal, which is further filtered out (detrended) using a low degree polynomial fit in the spherical reference frame. This detrending is a

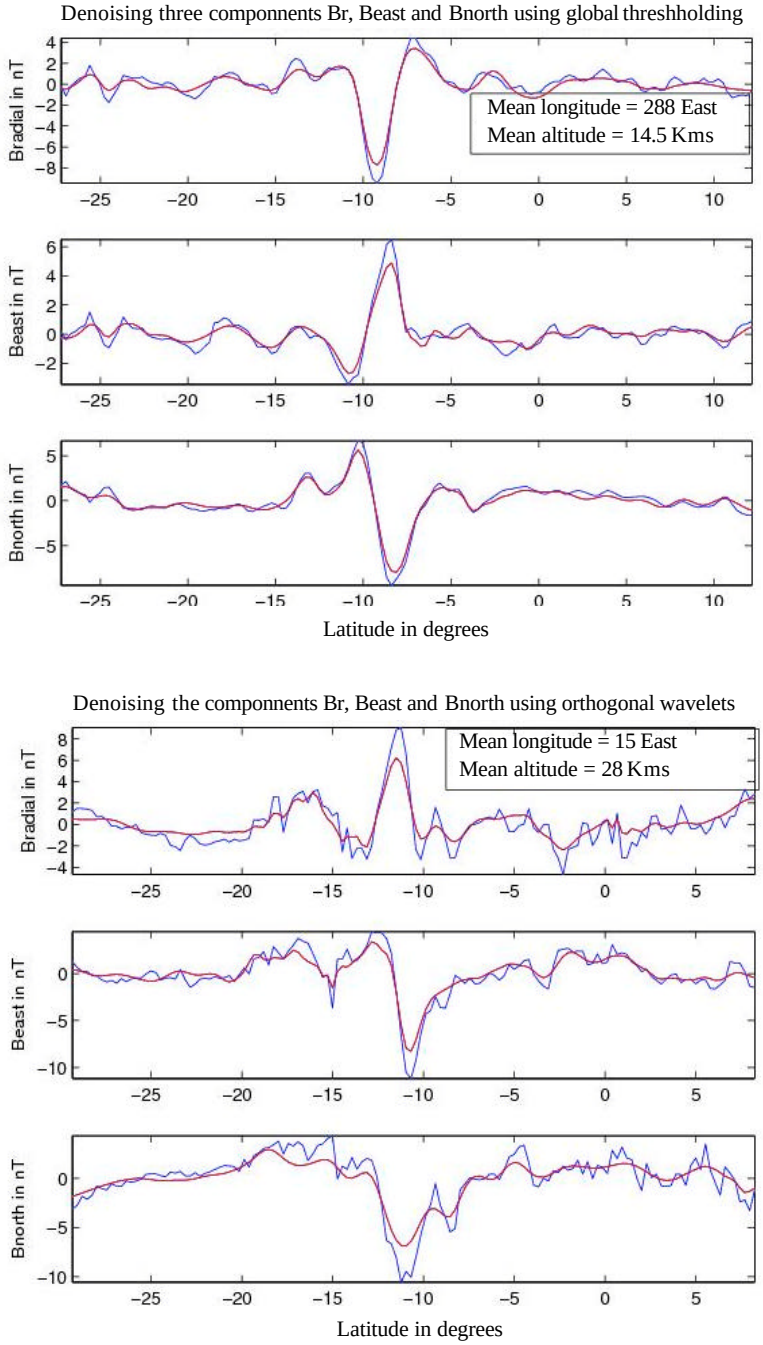

Fig. 1: Example of denoising magnetometer data using Daubechies orthogonal wavelets. Denoised data are plotted in red while initial raw data are in blue. The anomalies are superimposed to show the effectiveness of denoising to eliminate external field using wavelets. We use 20 coefficients (D20) of Daubechies wavelets

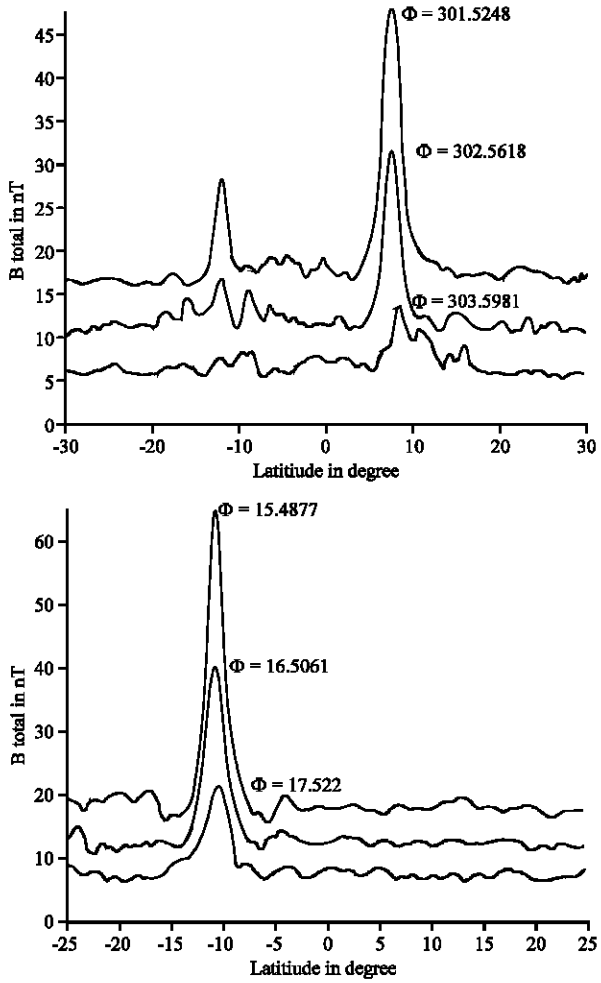

Fig. 2: Example of lunar magnetic anomalies. Lunar magnetic anomalies are repeated in adjacent tracks. (Top) Magnetic total components data over Reiner Gamma on January 27th 1999. (Bottom) Magnetic total components data over Descartes formations on April 13th 1999

common procedure in satellite magnetism. It was formerly used to reduce Apollo subsatellite magnetometer data (Hood *et al*., 1981), LP magnetometer data (Hood *et al*., 2001) and Mars Global Surveyor (MGS) magnetometer data (Hood *et al*., 2005). It is worth stressing that this empirical method generates long scale spurious effects (Thébault *et al*., 2008), but the obtained results in the lunar case may still be used with confidence as we focus on spatial scales smaller than the created artifacts.

The processing methods described earlier are applied to the whole selected half-orbits. A systematic visual inspection was carried out and the lunar remnant magnetic fields over a given area were considered to be genuine if they were repeatedly detected in close adjacent profiles. Figure 2 shows an example of the selected lunar magnetic field over Reiner Gamma and Descartes Formation. This processing was applied over the four regions of very high albedo: Reiner Gamma, Descartes Formation, Mare Marginis and Mare Ingenii. Corresponding results are plotted in Fig. 3 to 6. Table 1 and 2 compare some statistics between raw and processed data.

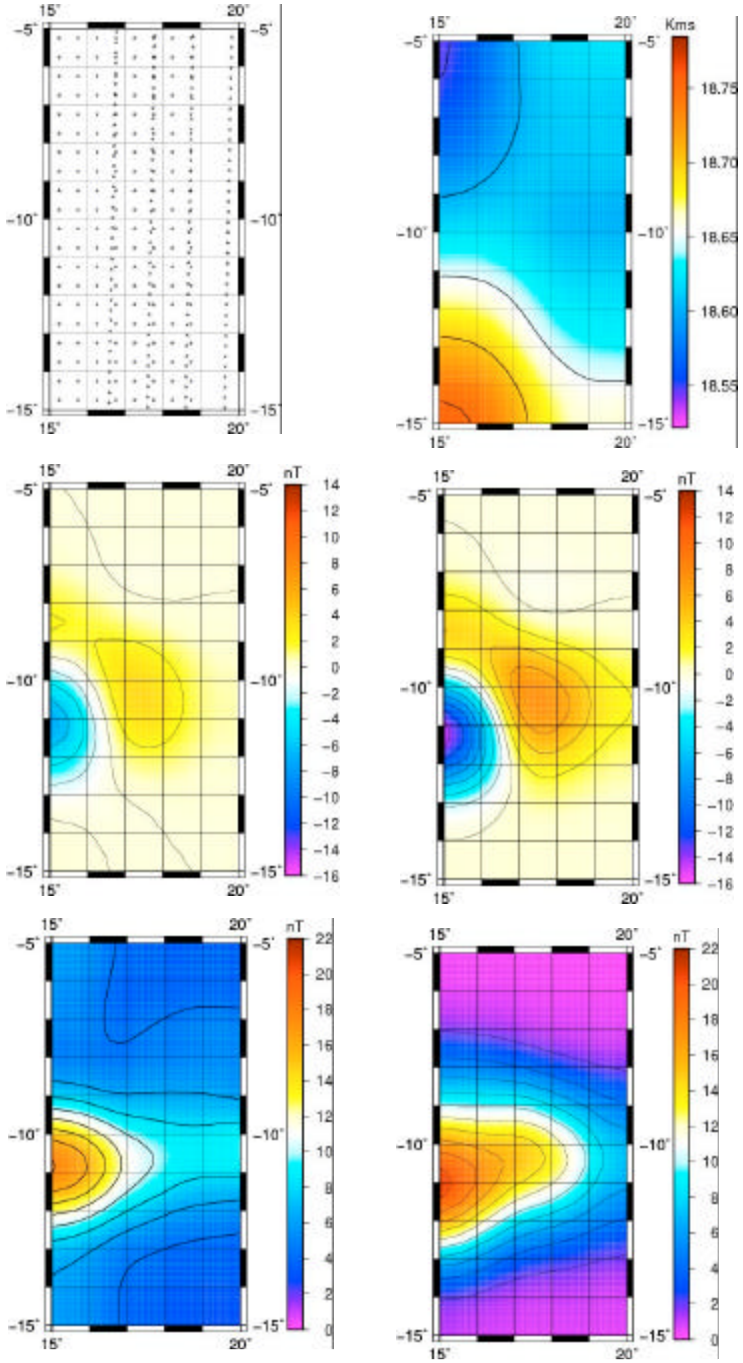

Fig. 3: Magnetic anomalies over Descartes Formation. (Top-Left) Data distribution. (Top-right) The altitude of the LP satellite expressed in km. (Middle-left) Radial component of the observed field. (Middle-right) Radial component of the modeled field. (Bottom-left) Total component of the observed field. (Bottom-right) Total component of the modeled field. The contour map of magnetic field is in nT. The projection system is the equidistant cylindrical centered on 16.5E

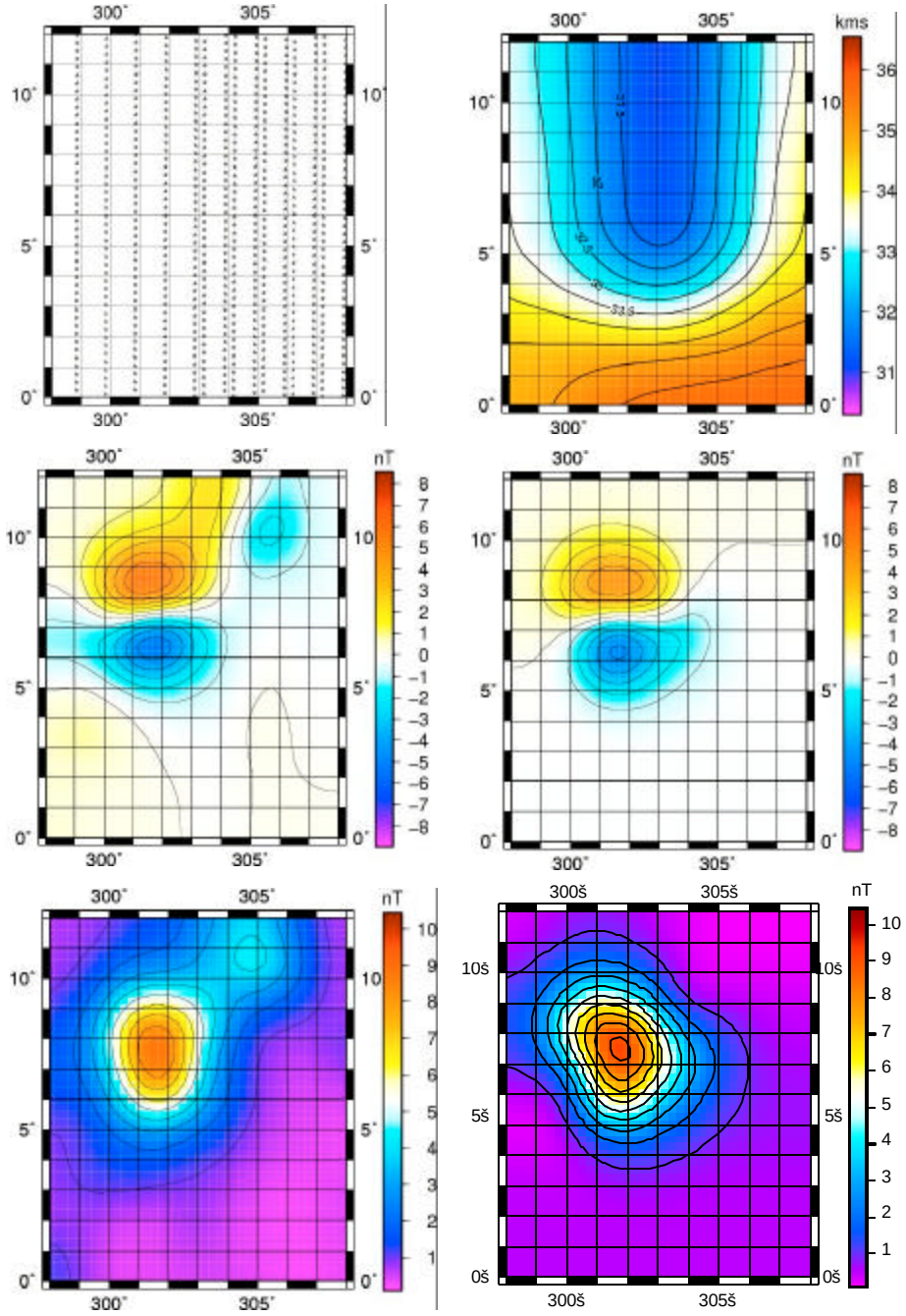

Fig. 4: Magnetic anomalies over Reiner Gamma Formation. (Top-Left) Data distribution. (Top-right) The altitude of the LP satellite expressed in km. (Middle-left) Radial component of the observed field. (Middle-right) Radial component of the modeled field. (Bottom-left) Total component of the observed field. (Bottom-right) Total component of the modeled field. The contour map of magnetic field is in nT. The projection system is the equidistant cylindrical centered on 302E

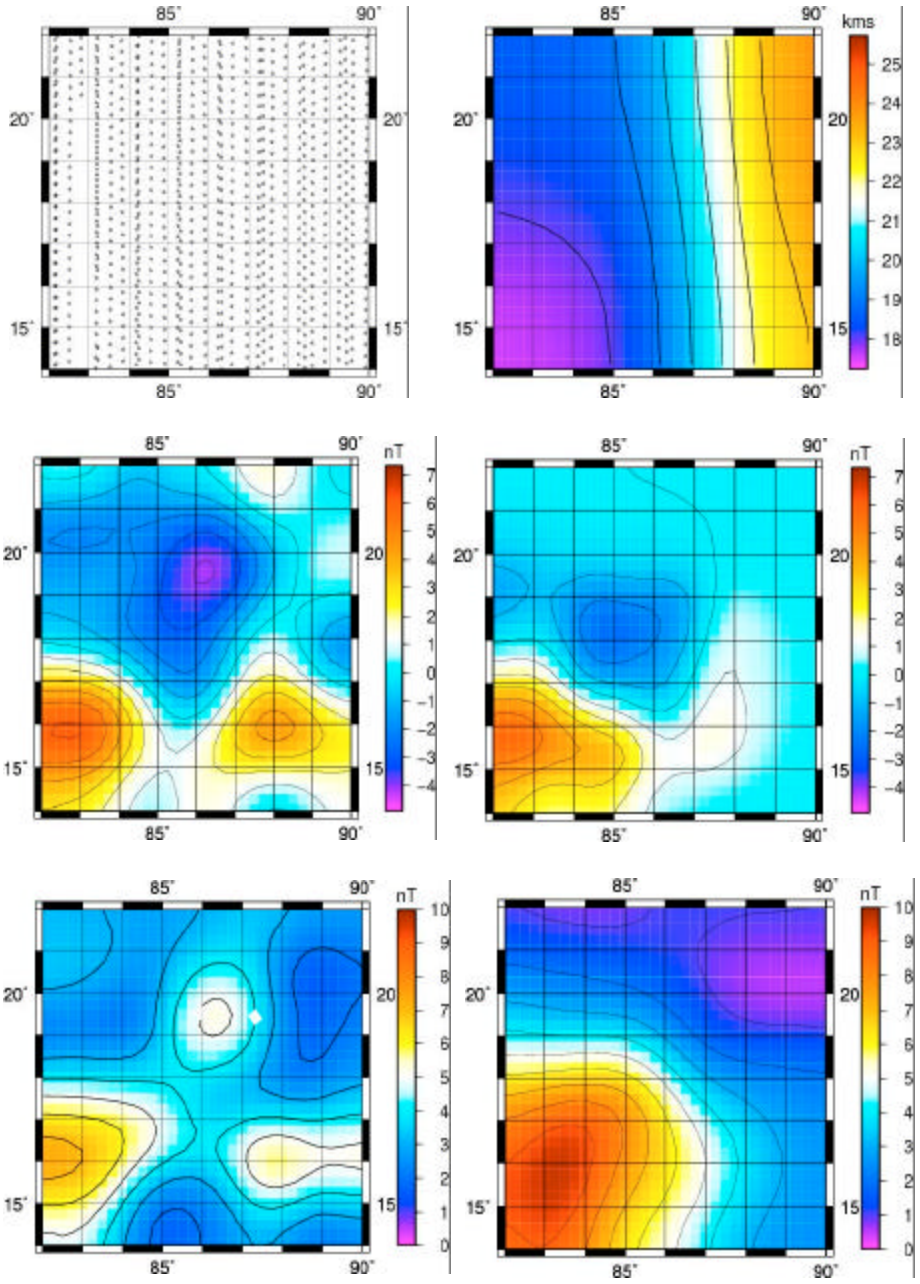

Fig. 5: Magnetic anomalies over Mare Marginis Formation. (Top-Left) Data distribution. (Top-right) The altitude of the LP satellite expressed in km. (Middle-left) Radial component of the observed field. (Middle-right) Radial component of the modeled field. (Bottom-left) Total component of the observed field. (Bottom-right) Total component of the modeled field. The contour map of magnetic field is in nT. The projection system is the equidistant cylindrical centered on 86E

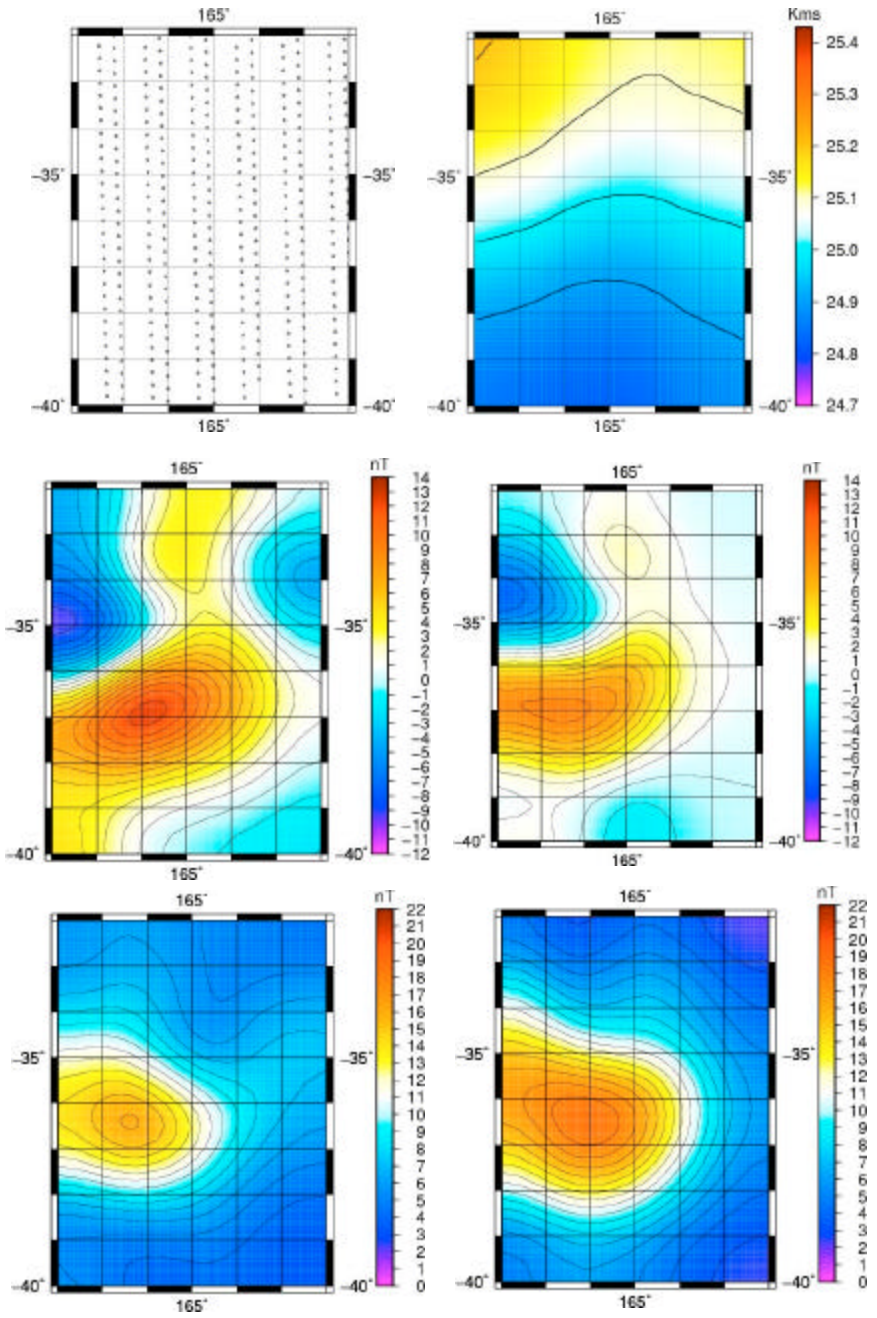

Fig. 6: Magnetic anomalies over Mare Ingenii Formation. (Top-Left) Data distribution. (Top-right) The altitude of the LP satellite expressed in km. (Middle-left) Radial component of the observed field. (Middle-right) Radial component of the modeled field. (Bottom-left) Total component of the observed field. (Bottom-right) Total component of the modeled field. The contour map of magnetic field is in nT. The projection system is the equidistant cylindrical centered on 168E

Table 1: Magnetic field anomalies statistics: Raw data

Formation	Component	Nb of data	Altitude range (km)		Anomaly range (nT)		Average (nT)	Standard dev (nT)
Descartes	Radial	863	18	40	-38	29	0.8	5.3
	Total	863	18	40	0	50	6.1	6.5
Reiner Gamma	Radial	783	18	40	-41	38	0.82	5.2
	Total	783	18	40	0	50	5.3	5.2
Mare Marginis	Radial	651	20	40	-9	18	0.1	6.1
	Total	651	20	40	0	19	3.6	1.8
Mare Ingenii	Radial	347	24	29	-14	20	1.6	5.4
	Total	347	24	29	2	23	8.6	4.8

Table 2: Magnetic field anomalies statistics: Processed data

Formation	Component	Nb of data	Altitude range (km)		Anomaly range (nT)		Average (nT)	Standard dev (nT)
Descartes	Radial	200	18	19	-24	15	0.03	0.5
	Total	200	18	19	3	31	0.03	4.7
Reiner Gamma	Radial	480	30	36	-8	8	0.01	0.2
	Total	480	30	36	0	10	0.01	2.1
Mare Marginis	Radial	240	17.5	25.5	-7	9	0.02	0.5
	Total	240	17.5	25.5	1	9	0.02	1.6
Mare Ingenii	Radial	192	24.5	25.5	-15	17	0.07	0.8
	Total	192	24.5	25.5	3	18	0.07	3.8

The radial component of the anomaly field over Reiner Gamma and Mare Ingenii shows a mainly NE-SW direction, whereas the Descartes and Mare Marginis anomalies are principally E-W (Fig. 3-6). The magnetic anomaly of the total field over Descartes Formation (Fig. 3) shows a maximum magnitude of 22 nT at (11S, 15.5E) that is in good agreement with the study of Richmond *et al*. (2003). This maximum intensity coincides with the area of highly marked albedo. Considering the radial component of the anomaly field, this marked albedo closely correlates with the negative lobe of the magnetic anomaly (Fig. 3). The Reiner Gamma total field anomaly shows two anomalies (Fig. 4): the strongest, about 16 nT, is centered over (7.5N, 301E) in the southern region and the weakest, of about 6 nT, lies in the northern part of the map. When comparing these results with those given by Hood *et al*. (2001) they are consistent for the anomaly direction but the magnitudes are lower. We explain this difference by the altitude variation between both data sets: altitude in this study varies from 30 to 35 km while it varies from 18 to 20 km in the study of Hood *et al*. (2001). Previous works, based on Apollo 15 and 16 subsatellite magnetometric data with almost the same altitude range (Hood *et al*., 1981), are more coherent with our processed data. The radial component of Reiner Gamma mapped in this research varies from -8 nT to +8 nT, which is slightly different from that mapped by Hood *et al*. (1981) using Apollo 16 (-3 to +10 nT), but both have the same direction. This is due firstly to the incomplete coverage of Apollo data over the same region compared to that of LP and secondly to the different high-pass filters used in each study. Similarly, Fig. 5 shows the magnetic anomaly over Mare Marginis which has a maximum about 7nT and is centered on (16N, 83E). This relatively strong anomaly has been previously reported by Hood and Schubert (1980) using the electron reflectance technique. At last, present results obtained for Mare Ingenii on the farside (Fig. 6) are coherent with those of Hood *et al*. (2001). Both total magnetic field maps reveal a maximum magnitude centered at (37.5S, 163.5E) coinciding also with the marked high albedo feature. This high albedo zone is completely included in the positive part of the dipole field (Fig. 6). These four high albedo regions, either in nearside or farside, also bear a comparatively strong magnetization with a mainly dipolar geometry at satellite altitude.

METHOD OF INVERSION

The dipolar geometry of the magnetic signal is adapted to a source modeling using an equivalent source of very simple geometry, like a disk uniformly magnetized at depth. In order to test the former

dynamo hypothesis, we assume that the four major magnetic anomalies discussed above were acquired in an ambient global dipole magnetic field. In general, we may use different approaches to determine the physical parameters of a magnetized body. The first one considers the forward method, which consists of setting an equivalent layer of dipoles within the crust (Hood *et al*., 2005, for MGS magnetic data). The parameters are then found by consecutive trials and comparisons between the magnetic field generated by the equivalent layer and the satellite data. In this research, considering the isolated and rather dipolar nature of the magnetic anomalies under study, we may use an inverse method as we assume unique sources for each of the four regions. The geometry and depths of sources are shown in Table 2. Moreover, the Lunar magnetic field is being assumed to be of remnant origin and the magnetization $\vec{M}$ of rocks is assumed to be aligned with the now extinct dipolar magnetic field that was imprinted in rocks 3.8 Ga ago (Imbrian age for the four structures under study). Present purpose is thus to estimate $\vec{M}$ in order to obtain an estimate of the angular location of the corresponding paleomagnetic poles. The method can be summarized as follows (Parker *et al*., 1987; Parker, 1991):

A source with magnetization $\vec{M}$ generates a magnetic field $\vec{B}(\vec{r})$ at any space location $\vec{r}$ through the equation (Blakely, 1996):

$$\vec{B}(\vec{r}) = -\vec{\nabla}_r \left\{ \frac{\mu_0}{4\pi} \int_v \vec{M}(\vec{r}_0) \bullet \vec{\nabla}_0 \frac{1}{|\vec{r} - \vec{r}_0|} dv \right\} \tag{1}$$

where, $\vec{\nabla}_r$ is the gradient operator with respect to the observation coordinates, $\vec{\nabla}_0$ is the gradient operator with respect to the source coordinates, v is the volume of the magnetized body, μ_0 is the magnetic permeability of free space and (r_0, θ_0, ϕ_0) are the spherical coordinates of the elementary point source. We may express the total magnetic anomaly at any point r_j as a scalar product:

$$\vec{B}(\vec{r}_j) = \left\langle \vec{e}_0, \vec{B}(\vec{r}_j) \right\rangle = \int_v \vec{G}_j(\vec{r}_0) \bullet \vec{M}(\vec{r}_0) dv \tag{2}$$

where, $\vec{e}_0$ is the unit vector in the direction of $\vec{B}(\vec{r}_j)$ and $\vec{G}$ is the vector-valued Green's function given by Parker (1991):

$$\vec{G}_j(\vec{r}_0) = \frac{\mu_0}{4\pi} \left\{ \frac{3(\vec{r}_j - \vec{r}_0) \bullet \vec{e}_0 (\vec{r}_j - \vec{r}_0)}{\|\vec{r} - \vec{r}_0\|^5} - \frac{\vec{e}_0}{\|\vec{r}_j - \vec{r}_0\|^3} \right\} \tag{3}$$

Comparisons between the observed $\vec{B}^{obs}$ and the modeled $\vec{B}^{mod}$ fields in the studied area may be achieved in the least-square sense by minimizing the Euclidean norm Q^2:

$$Q^2 = \left\| \vec{B}^{mod}(\vec{r}_j) - \vec{B}^{obs}(\vec{r}_j) \right\|^2 \tag{4}$$

Solution non uniqueness is a ubiquitous problem in geomagnetism. A further constraint is then added to the inverse problem and we assume the magnitude of magnetization $\vec{M}$ to be higher than the minimum value given by Parker (2003):

$$M \geq M_0 = \frac{1.4491 \|B_{max}\| / \mu_0}{\ln(h_2 / h_1)} \tag{5}$$

where, $||B_{max}||$ is the maximum total magnetic anomaly observed, h_1 is the altitude and h_2 is the altitude plus layer thickness. This equation was first established by Parker (2003) in the case of crustal remnant magnetization on Mars and was recently applied by Nicholas *et al*. (2007) on the Moon.

From the least-squares estimation of the magnetization vector parameter (M_r, M_θ, M_ϕ) we deduce the selenographic angular location of the paleomagnetic poles. The latitude of paleo-pole λ_p is given by Butler (1992):

$$\lambda_p = \sin^{-1}(\sin\lambda_0 \cos\beta + \cos\lambda_0 \sin\beta \cos D) \tag{6}$$

where, λ_0 is the source latitude, D is the declination angle derived from $D = \tan^{-1}(-M_\theta/M_\phi)$ and I is the dip angle given by

$$I = \tan^{-1}\left(-\frac{M_r}{\sqrt{(M_\theta^2 + M_\phi^2)}}\right)$$

and the co-latitude β is given by $\beta = \tan^{-1}(2/\tan I)$. The longitudinal difference between the pole and the source location is positive toward the east and is given by:

$$\Delta\phi = \sin^{-1}(\sin\beta \sin D / \cos\lambda_p) \tag{7}$$

If $\cos\beta \geq \sin\lambda_0 \sin\lambda_p$ then the longitude of the paleo-pole is evaluated using $\phi_p = \phi_0 + \Delta\phi$ where ϕ_0 is the source longitude, otherwise, $\phi_p = \phi_0 + 180° + \Delta\phi$.

Following Butler (1992), present results are determined with the semi-axes confidence ellipse error in paleo-pole locations given by:

$$dp = \alpha_{95}\left(\frac{1 + 3\cos^2\beta}{2}\right) \tag{8}$$

And:

$$dm = \alpha_{95}\left(\frac{\sin\beta}{\cos I}\right) \tag{9}$$

where, α_{95} is the 95% confidence error taken to be equal to the standard deviation.

RESULTS AND DISCUSSION

Using the source geometry parameters in Table 3, we find computed magnetic fields rather similar to the observed ones. For the Reiner Gamma, Descartes Formation, Mare Marginis and Mare Ingenii, the iterative procedure described above shows residual mean square misfits between the computed and measured field equal to 2.45, 3.02, 2.25 and 2.95 nT, respectively. The depth of the sources ranges between 10 and 20 km, which is in accordance with earlier study (Hood *et al*., 2001; Nicholas *et al*., 2007). Source anomaly is assumed to be near the surface. The estimated magnetization value of Reiner Gamma, 0.12 Am^{-1}, is close to the corresponding value given by Nicholas *et al*. (2007) using also an ideal body as given by Eq. 5. Magnetization intensity values obtained for Descartes Formation and Mare Marginis are close to each other. The Mare Ingenii feature shows a small value compared to the others. This may be related to the demagnetizing effects of the more heavily cratered farside to which it belongs and to the large extension of the formation.

The pole positions of the hypothetical global field are derived from the magnetization vectors of the source using Eq. 6 and 7. The results are given in Table 4 and are shown in Fig. 7. This figure shows that the pole positions are located in the farside and are clustered around the position (30S, 215E). However, Mare Ingenii exhibits an equatorial pole position slightly further from the cluster center. In addition, the inverse modeling result showed a higher sensitivity to the initial priory information. This singular behavior may be related to its location within the farside of the Moon or to the fact that the simple assumptions used in this study are less reasonable for Mare Ingenii. It is worth stressing that the magnetized crustal material or Mare Ingenii may have been reworked by heavy meteoric bombardment during geological history. Moreover, it is generally accepted that Mare Ingenii is associated with an antipodal young basin impact (Hood *et al*., 2001). Conversely, Reiner Gamma, Descartes Formation and Mare Marginis, belonging to the nearside of the Moon, are not close to each other. The physical conditions are thus rather different, although the common parameter for these four formations is their Imbrian age. Taking the above results with the necessary caution, a cluster of paleomagnetic positions is a good indicator that the Moon once had in its early age a global dipolar core field.

Table 3: Magnetization properties deduced from equivalent source

Formation	Disk center coordinates		Disk radii	Disk thickness	Magnetization (Am^{-1})
Descartes	10.5S	16E	60 km	10 km	0.083
Reiner Gamma	7.5.N	30.51E	45 km	10 km	0.122
Mare Marginis	13N	86E	65 km	20 km	0.081
Mare Ingenii	36.5S	163.5E	100 km	10 km	0.043

Table 4: Directional properties of paleo-poles. All units are in degrees

Formation	Inclination	Declination	Pole coordinates		Error α_{95}	Ellipse axis dp	Ellipse axis dm
Descartes	-48	243	17S	251E	39	22	45
Reiner Gamma	+22	206	50S	241E	19	11	23
Mare Marginis	-33	120	30S	190E	21	12	25
Mare Ingenii	-33.5	192	13S	195E	23	15	35

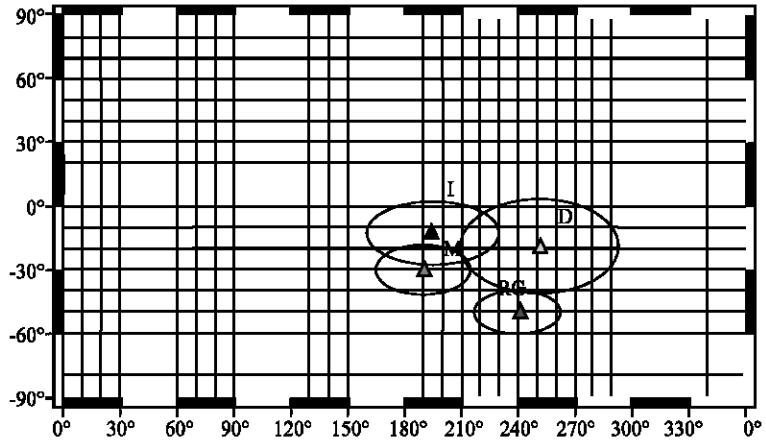

Fig. 7: The location of lunar paleomagnetic poles mapped in the equidistant cylindrical projection centred at 180E. The projection shows adjacent locations of the paleomagnetic poles for the formations computed according to Eq. 6 and 7. RG: for Reiner Gamma, D for Descartes Formation, M for Mare Marginis and I for Mare Ingenii. The 95% confident ellipse is computed using Eq. 8 and 9

CONCLUSION

We have mapped magnetic anomalies over four lunar regions of high albedo using selected orbits with low noise. The mapping field is consistent and presents real lunar crustal sources. The study of the lunar magnetic pole positions of these selected high albedo formations of a similar age uses an inversion method based on simple uniformly magnetized circular disks. This inversion is slightly sensitive to source position, especially when the anomaly shape is far from being dipolar. However, our results show a clustering of poles as determined by the magnetization vectors associated to these strong lunar magnetic anomalies. Moreover, these pole positions belonging to southern part of the farside are partially in favor of a magnetization acquired in the presence of a lunar magnetic field generated by a global paleo-dynamo. However, it currently remains difficult to expand our conclusions to the global Moon's crustal magnetization. We intend in the future to generalize the modeling and to investigate the magnetization of all significant lunar magnetic anomalies using a more complex geometry form for the causative sources. In order to process the data at global scales, we will need to consider a more extensive set of LP data, like those at low altitudes and acquired in different Moon environments. This will help us assessing the correlation between albedo, geological age and magnetization in a more statistical sense. In addition, a re-examination of returned samples from the Apollo mission will also help in better understanding the magnetic evolution that took place during the Moon's early history.

ACKNOWLEDGMENTS

We are grateful to anonymous referees for their very constructive comments. Steven Joy (Institute of Geophysics and Planetary Physics IGPP/UCLA) is greatly acknowledged for making Lunar Prospector magnetic data available to us. For IPGP, this is contribution number 2345.

REFERENCES

Andolz, F.J., T.A. Daugherty and A.B. Binder, 1998. Lunar Prospector Mission Handbook. Lockheed Martin Missile and Space Co.

Binder, A., 1998. Lunar prospector: Overview. Science, 281: 1475-1476.

Blakely, R.J., 1996. Potential Theory in Gravity and Magnetic. Cambridge University Press, Cambridge.

Blewett, D., B. Ray and P.G. Lucey, 2005. Lunar optical maturity investigation: A possible recent impact crater and a magnetic anomalies. J. Geophys. Res., 110, E04015, doi: 10.1029/2004JE002380.

Butler, R.F., 1992. Paleomagnetism: Magnetic Domains to Geologic Terranes. Blackwell Sci, Malden Mass.

Cisowski, S.M., D.W. Collinson, S.K. Runcorn, A. Stephenson and M. Fuller, 1983. A review of lunar paleointensity data and implication for the origin of lunar magnetism. J. Geophys. Res., 88: 691-704.

Collinson, D.W., 1993. Magnetism of the Moon-a lunar core dynamo or impact magnetization? Surveys Geophys., 14 (1): 89-118.

Daubechies, I., 1992. Ten lectures in wavelets. CBMS-NSF Lecture Notes, 61, SIAM.

Dyal, P., C.W. Parkin and W.D. Daily, 1974. Magnetism and the Interior of the Moon. Rev. Geophys. Space Phys., 12: 568-591.

Fedi, M. and T. Quarta, 1998. Wavelet analysis for the regional-residual and local separation of potential field anomalies. Geophys. Prospect., 46: 507-525.

Fuller, M., 1974. Lunar magnetism. Rev. Geophys. Space Phys., 12: 23-70.

Fuller, M. and S. Cisowski, 1987. Lunar Paleomagnetism. In: Geomagnetism, Jacobs, J.(Ed.). Academic Press, CA., pp: 307-456.

Halekas, J.S., D.L. Mitchell, R.P. Lin, S. Frey, L.L. Hood, M.H. Acuña and A.B. Binder, 2001. Mapping of crustal magnetic anomalies on the lunar near side by lunar prospector electron reflectometer. J. Geophys. Res., 106: 27481-27852.

Halekas, J.S., D.L. Mitchell, R.P. Lin, L.L. Hood, M.H. Acuna and A.B. Binder, 2002. Demagnetization signatures of lunar impact craters. Geophys. Res. Lett., 29 (13): 13-1645 10.1029/2001GL013924.

Hood, L.L. and G. Schubert, 1980. Lunar magnetic anomalies and surface optical properties. Science, 208: 49-51.

Hood, L.L., C.T. Russell and P.J. Coleman Jr., 1981. Contour maps of the lunar remanent magnetic fields. J. Geophys. Res., 86: 1055-1069.

Hood, L.L. and Z. Huang, 1991. Formation of magnetic anomalies antipodal to lunar impact: Two-dimensional model calculations. J. Geophys. Res., 96 (6): 9837-9846.

Hood, L.L., D.L. Mitchel, R.P. Lin, M.H. Acuña and A. Binder, 1999. Initial measurements of the lunar induced magnetic dipole moment using lunar prospector magnetometer data. Geophys. Res. Lett., 26: 2327-2331.

Hood, L.L., A. Zakharian, J.S. Halekas, D.L. Mitchell, R.P. Lin, M.H. Acuña and A.B. Binder, 2001. Initial mapping and interpretation of lunar crust magnetic anomalies using lunar prospector magnetometer data. J. Geophys. Res., 106: 27825-27839.

Hood, L.L., C.N. Young, N.C. Richmond and K.P. Harrison, 2005. Modeling of major martian magnetic anomalies: Further evidence for polar reorientations during the Noachian. Icarus, 177: 144-173.

Hood, L.L. and N.A. Artemieva, 2008. Antipodal Effect of Lunar Basin-Forming Impacts: Initial 3D Simulations and Comparisons with Observations. Icarus, Submitted.

Khan, A., K. Mosegaard, J.G. Williams and P. Lognonné, 2004. Does the Moon posses a molten core? Probing the deep lunar interior using results from LLR and Lunar Prospector. J. Geophys. Res., 109, doi: 1092/2004JEOO2294.

Leblanc, G.E. and W. Morris, 2001. De-noising of aeromagnetic data via wavelet transform. Geophysics, 66: 1793-1804.

Lin, R.P., D.L. Mitchell, D.W. Curtis, K.A. Anderson, C.W. Carlson, J. McFadden, M.H. Acuna, L.L. Hood and A.B. Binder, 1998. Lunar surface magnetic fields and their interaction with the solar wind: Results from lunar prospector. Science, 281: 1480-1484.

Ness, N.F., 1971. Interaction of the Solar Wind with the Moon. Solar Terrestrial Phys., pp: 159-205.

Nicholas, J.B., M.E. Purucker and T.J. Sabaka, 2007. Age spot or youthful marking: The origin of Reiner Gamma. Geophys. Res. Lett., 34, doi:1029/2006GL027794.

Parker, R.L., L. Shure and J.A. Hildebrand, 1987. The application of inverse theory to seamount magnetism. Rev. Geophys., 25: 17-40.

Parker, R.L., 1991. A Theory of Ideal bodies for seamount magnetism. J. Geophys. Res., 96: 16101-16112.

Parker, R.L., 2003. Ideal bodies for Mars magnetics. J. Geophys. Res., 108: 5006, doi: 10.1029/2001JE001760.

Richmond, N.C., L.L. Hood, J.S. Halekas, D.L. Mitchell, R.P. Lin, M.H. Acuña and A.B. Binder, 2003. Correlation of a strong lunar magnetic anomalies with high-albedo region of descartes mountains. Geophys. Res. Lett., 30 (7): 1395, doi:10.1029/2003GL016938.

Richmond, N.C., L.L. Hood, J.S. Halekas, D.L. Mitchell, R.P. Lin, M.H. Acuña and A.B. Binder, 2005. Correlation between magnetic anomalies and surface geology antipodal to lunar impact basins. J. Geophys. Res., 110, doi:10.1029/2005JE002405.

Schultz, P.H. and L.J. Snrka, 1980. Cometary collisions on the Moon and Mercury. Nature, 284: 22-26.

Thébault, E., V. Lesur and M. Hamoudi, 2008. The shortcomings of the along track satellite filtering in geomagnetism. J. Geophys. Int. (Submitted).